Reactions of Ar^+, Ne^+, and He^+ with SiF_4 from thermal energy to 50 eV c.m.

M. E. Weber
Department of Chemistry, University of California, Berkeley, California 94720

P. B. Armentrout[a)]
Department of Chemistry, University of Utah, Salt Lake City, Utah 84112

(Received 1 September 1988; accepted 7 November 1988)

Guided ion-beam techniques are used to measure the cross sections for reaction of SiF_4 with Ar^+, Ne^+, and He^+ from thermal to 50 eV. Charge transfer followed by loss of F atoms are the sole processes observed. All SiF_x^+ ($x = 0$–4) products are observed, except for SiF_4^+ from reaction with Ne^+ and He^+, and Si^+ from reaction with Ar^+. At high energies, the dominant products are SiF_3^+ in the Ar system, and SiF^+ in both the Ne and He systems. There is some evidence in the Ne system for an excited state of SiF_3^+ at 5.7 eV. In the Ar^+ and Ne^+ reactions, the observed energetics are consistent with literature thermochemistry, but with He^+, reaction barriers are observed. A value of $\Delta H^0_{f,298}(SiF_3^+) = -30.1 \pm 0.9$ kcal/mol is derived, which is in agreement with previous values but is much more precise. The observed product distributions and energetics are explained by consideration of the potential energy surfaces and the difference in ionization potentials of the rare gases. Finally, the relationships of these reactions to plasma deposition and etching are discussed.

INTRODUCTION

An important tool in the fabrication of microelectronic devices is the use of plasmas to etch and deposit silicon, silicon oxide, and silicon nitride layers. Understanding of the chemical mechanisms involved can provide insight into the most important physical parameters of a plasma reactor and the optimum starting materials. Although neutral species dominate the gas-phase composition in a plasma system, the rates for ion–molcule reactions are generally much greater than for the neutral reactions due to the strong long-range forces present. Thus ion–molecule reactions have significant effects on plasma composition[1–3] and hence the resulting plasma process.

Rare gases (Rg) are used frequently in plasma systems. In deposition processes, the starting material often consists of up to 90% rare gas diluents, in addition to the reactive gas. Although these diluents were initially believed to be inert, the amount and identity of the diluent has been found to significantly affect silane[4] and disilane[5] deposition characteristics. Specifically, films produced with He and Ne as the diluent gas have markedly different film properties and deposition rates than films where Ar and Kr are present. These differences are proposed to be due to an increase in the SiH_x^+ ion density caused by reactions involving excited states of the rare gas.[4] In the case of etching, energetic (1 keV) rare gas ions are often used in tandem with reactive neutral species, such as fluorides, to symbiotically enhance the etch rates and the directionality of the etched features.[6–8] The etch rate is highly dependent on the ion used (Ar^+, Ne^+, or He^+), yet the reasons for this dependency are unknown.[8]

The study of rare gas ion–molecule reactions related to silicon etching and deposition plasmas has been the focus of recent work. In one study, the reaction rates of SiH_4 with Ar^+, Ne^+, and He^+ were measured in the interaction energy range of ~0.04 to 1 eV using the drift tube technique.[9] For He^+ and Ne^+, the total charge exchange rates were fast, ~95% and 60% of the collision rate, respectively. However, that for Ar^+ was substantially slower, proceeding at only 1% of the Langevin rate. This enormous discrepancy cannot be explained on thermodynamic grounds, since dissociative charge transfer to form SiH_n^+ ($n = 0$–3) is exothermic for all three rare gases.[10] This observation supports the explanation mentioned above for the marked differences found in films produced with Ar and Kr as the diluent compared with He and Ne.[4] In other studies, cross sections for reaction of CF_4 with He^+ and Ne^+ have been measured at high energies (700 to 5000 eV),[11] and drift tube techniques have been used to determine thermal reaction rates.[12] Also, UV emissions from the $CF_4 + Rg^+$ interactions have been measured at collision energies of 1–1800 eV (Rg = He, Ne, Ar)[13] and 1–25 keV (Rg = He, Ne).[14]

Many plasma systems involve SiF_4 as either starting material[15,16] or as a volatile product from surface reactions, and thus reactions involving SiF_4 are of particular interest. Recent work in our laboratories focused on the mechanisms involved in the reaction of Si^+ with SiF_4.[17] Also, the thermochemistry of the resulting SiF_x and SiF_x^+ products, which had uncertainties of as much as 20 kcal/mol, was derived and compared to literature values. The present work is a continuation of this previous work, and is motivated by the likely importance of both rare gas and SiF_4 reactions in plasma systems.

Reaction thermochemistry

For the reaction of rare gas ions with tetrafluorosilane, there are five energetically accessible SiF_x^+ product ions in the energy range studied here, as given in reactions (1):

$$Rg^+ + SiF_4 \rightarrow SiF_4^+ + Rg \qquad (1a)$$

[a)] NSF Presidential Young Investigator, 1984–1989; Alfred P. Sloan Fellow; Camille and Henry Dreyfus Teacher–Scholar, 1988–1993.

 0021-9606/89/042213-12$02.10

TABLE I. Heats of formation at 298 K (kcal/mol).[a]

Species	$\Delta H^0_{f,298}$	Species	$\Delta H^0_{f,298}$
Si^+	297.1 ± 1.0[b]	F	18.97 ± 0.07[c]
SiF^+	170.4 ± 2.2[b]	F^+	422.28 ± 0.07[c]
SiF_2^+	109 ± 2[b]	He^+	568.48[c]
SiF_3^+	−26.2 ± 4.7[b]	$Ne^+(^2P_{3/2})$	498.98[c]
	−30.1 ± 0.9[d]	$Ne^+(^2P_{1/2})$	501.22[c]
SiF_4^+	−19.94 ± 0.50[e]	$Ar^+(^2P_{3/2})$	364.91[c]
SiF	−5 ± 3[b]	$Ar^+(^2P_{1/2})$	369.00[c]
SiF_2	−141 ± 2[b]		
SiF_3	−258 ± 3[b]		
SiF_4	−386.0 ± 0.2[b]		

[a]Ion heats of formation are calculated using the convention that the electron is a monatomic gas. This convention is adopted in the JANAF tables (Ref. 18). Values compared from the literature which use the "stationary electron" convention should be increased by 1.48 kcal/mol at 298 K.
[b]Recommended values from Ref. 17.
[c]Reference 18.
[d]This work.
[e]Calculated using $IP(SiF_4) = 15.81 \pm 0.02$ (P. J. Bassett and D. R. Lloyd, J. Chem. Soc. A **1971**, 641).

$$\rightarrow SiF_3^+ + F + Rg \quad (1b)$$

$$\rightarrow SiF_2^+ + [F + F] + Rg \quad (1c)$$

$$\rightarrow SiF + [F + F] + F + Rg \quad (1d)$$

$$\rightarrow Si^+ + [F + F] + [F + F] + Rg. \quad (1e)$$

In processes (1c) through (1e), fluorine can conceivably be liberated as either molecular fluorine or separated atoms. This possibility is indicated by brackets. Expected reaction enthalpies are determined using the recommended SiF_x^+ thermochemistry given in our recent study of the reaction of Si^+ with SiF_4,[17] along with $\Delta H^0_{f,298}(Rg^+)$ values taken from the JANAF tables.[18] These heats of formation are tabulated in Table I. Table II gives the resulting reaction enthalpies for processes (1) for the Ar, Ne, and He rare gases.

Collision cross sections

The collision cross section σ_{col} for ion–molecule reactions at low energies is predicted by the Langevin–Gioumousis–Stevenson (LGS) model,[19]

$$\sigma_{LGS} = \pi e(2\alpha/E)^{1/2}, \quad (2)$$

where E is the interaction or center-of-mass (c.m.) energy of the reactants, e is the electronic charge, and α is the polarizability of the target molecule SiF_4. The value for $\alpha(SiF_4)$ is not well established, but it has been measured as 3.32 Å^3,[20] and can be calculated as 4.3 ± 0.4 Å^3 using the empirical method of Miller and Savchik.[21,22]

At high energies, σ_{col} for charge–transfer reactions may be best represented by the hard-sphere limit, given by

$$\sigma_{HS} = \pi R^2, \quad (3)$$

with R roughly estmated by $r_e(Rg–F^+) + r_e(F_3Si–F)$. For $F_3Si–F$, r_e has been measured as 1.552 Å.[23] The r_e for NeF^+ has been calculated as 1.465[24] and 1.65 Å,[25] to yield an average value of 1.56 Å. In the latter study, $r_e(HeF^+) = 1.33$ Å was also calculated.[25] An estimate for $r_e(ArF^+) = 2.0$ Å is obtained by comparing $r_e(NeF^+) = 1.56$ Å to the ratio of $r_e(ArH^+)$ and $r_e(NeH^+)$.[26] An analogous estimate for $r_e(HeF^+)$ yields 1.2 Å which is in good agreement with the calculated value. Thus the values used for R for the Ar, Ne, and He systems are 3.6, 3.1, and 2.8 Å, respectively, which result in $\sigma_{HS}(Ar^+–SiF_4) = 40.7$ Å^2, $\sigma_{HS}(Ne^+–SiF_4) = 30.2$ Å^2, and $\sigma_{HS} = (He^+–SiF_4) = 24.6$ Å^2. In this work, σ_{col} is taken to be the maximum of σ_{LGS} and σ_{HS}. Assuming the value of 3.32 Å^3 for $\alpha(SiF_4)$, $\sigma_{HS} = \sigma_{LGS}$ occurs at 0.57 eV for Ar^+, at 1.0 eV for Ne^+, and at 1.6 eV for He^+.

EXPERIMENT

General

The ion beam apparatus and experimental techniques used in this work are described in detail elsewhere.[27] The rare gas ions are produced as described below. The $^4He^+$, $^{20}Ne^+$, and $^{40}Ar^+$ ions are each mass analyzed and decelerated to the desired translational energy. The ion beam is injected into an rf octopole ion beam guide,[28] which passes through the reaction cell containing the SiF_4 reactant gas. The octopole beam guide utilizes rf electric fields to create a potential well which traps ions in the radial direction without affecting their axial energy. The pressure of SiF_4 is maintained sufficiently low, 0.02 to 0.2 mTorr, so that multiple ion–molecule collisions are improbable. The unreacted rare gas and product ions drift out of the gas chamber to the end of the octopole, where they are extracted and analyzed in a quadrupole mass filter. Finally, ions are detected by a sec-

TABLE II. Reaction thermochemistry at 298 K (eV).[a]

Process	Products	Rg = Ar	Rg = Ne	Rg = He	Uncertainty
(1a)	$SiF_4^+ + Rg$	+0.05	−5.76	−8.78	±0.02
(1b)	$SiF_3^+ + F + Rg$	+0.60	−5.21	−8.23	±0.2
(1c)	$SiF_2^+ + 2F + Rg$	+7.29	+1.48	−1.54	±0.09
(1c)	$SiF_2^+ + F_2 + Rg$	+5.64	−0.17	−3.19	±0.09
(1d)	$SiF^+ + 3F + Rg$	+10.77	+4.97	+1.94	±0.10
(1d)	$SiF^+ + F_2 + F + Rg$	+9.12	+3.32	+0.29	±0.10
(1e)	$Si^+ + 4F + Rg$	+17.09	+11.28	+8.26	±0.04
(1e)	$Si^+ + 2F_2 + Rg$	+13.80	+7.99	+4.97	±0.04

[a]For the $J = 3/2$ ground state of the Rg^+ ions.

ondary electron scintillation ion counter using standard pulse counting techniques. Raw ion intensities are converted to absolute reaction cross sections as described previously.[27]

Ion source

The rare gas ions are produced by electron impact of helium, neon, or argon gas, which have ionization potentials (IP) of 24.580, 21.559, and 15.755 eV, respectively.[29] The first excited electronic states of the ion are 65.4 eV for helium, 48.5 eV for neon, and 29.3 eV for argon above the neutral ground state.[29] Thus, to prevent formation of ionic excited states, the nominal electron energies used are 60, 41, and 20 eV, respectively. The electron energy distribution has a spread of less than ± 1 eV in each case. Only the $^2S_{1/2}$ ground state of He^+ is formed, but both the $^2P_{3/2}$ and $^2P_{1/2}$ spin–orbit states of Ne^+ and Ar^+ are produced, presumably with a 2:1 statistical population. The $^2P_{1/2}$ states of Ne^+ and Ar^+ lie 0.097 and 0.178 eV, respectively, above the $^2P_{3/2}$ ground states.[29]

Energy scale

Laboratory ion energies (lab) are converted to energies in the center-of-mass frame (c.m.) by using the conversion $E(\text{c.m.}) = E(\text{lab}) \times M/(m+M)$, where m is the ion mass and M is the target molecule mass.[27] This conversion factor is 0.96 for the He^+ reactions, 0.84 for the Ne^+ reactions, and 0.72 for the Ar^+ reactions. Unless stated otherwise, all energies quoted in this work correspond to the c.m. frame. The absolute energy scale and the corresponding full width at half-maximum (FWHM) of the ion kinetic energy distribution is determined by using the octopole beam guide as a retarding potential analyzer.[27] An accurate determination is possible since the interaction region and energy analysis region are physically the same. In this work, the uncertainty in the absolute energy scale is ± 0.05 eV (lab). The distribution of ion energies have an average FWHM of 0.3 eV for He^+, 0.4 eV for Ne^+, and 0.2 eV for Ar^+. At very low energies, the slower ions in the ion beam energy distribution are not transmitted through the octopole, which results in a narrowing of the ion energy distribution. We take advantage of this effect to access very low interaction energies as described previously.[27] Energies in data plots are mean ion energies which take into account this truncation of the ion beam distribution.

Ion collection efficiency

For charge transfer reactions, products may be formed through a long-range electron jump such that little or no forward momentum is transferred to the ionic products.[30] In such a case, up to 50% of these ions may have no forward velocity in the laboratory and will not drift out of the octopole to the detector. Furthermore, slow product ions which do transverse the octopole may be inefficiently transmitted through the quadrupole mass filter.[27] Cross section features and magnitudes for exothermic or nearly thermoneutral reactions channels, in particular, were indeed found to be sensitive to the extraction and focusing conditions following the octopole.

The cross section results presented here represent the averages of several determinations taken at different times over the course of a year. These results were the most reproducible and had the largest magnitudes for all products. Based on reproducibility, the uncertainty in the absolute cross sections is estimated as 60%, while the relative error is about 20%. Since ion collection may be incomplete, for reasons given above, it is possible that the actual cross sections might be as high as a factor of 2 greater than those reported. We do not believe this to be true, however, since other measurements in our laboratories of exothermic charge transfer processes are in good agreement with literature results.[27,31] In the present work, absolute cross sections as small as 10^{-2} Å^2 are measured.

Thermochemical analysis

The threshold regions of endothermic reactions are analyzed using the empirical model in Eq. (4),

$$\sigma_T(E) = \sigma_0[(E-E_T)^n/E^m], \tag{4}$$

where E_T is the translation energy, σ_0 is an energy independent scaling factor, and n and m are variable parameters. This general form has been discussed previously.[32,33] As in earlier studies, we have chosen to restrict the form of Eq. (4) to $m=1$, a form predicted for translationally driven reactions.[34] Furthermore, with $m=1$, Eq. (3) has been found to be quite useful in describing the shapes of endothermic reaction cross sections and in deriving accurate thermochemistry from the threshold energies for a wide range of systems. These systems include a related reaction with tetrafluorosilane,[17] reactions of silane and silicon hydrides,[35] and reactions of atomic transition metals with H_2, D_2,[36] and hydrocarbons.[33]

A complication here involves the treatment of the Ar^+ and Ne^+ data, which result from $J=3/2$ and $J=1/2$ spin–orbit states of the reactant ion. This is handled by an explicit sum over the contributions of the individual states, weighted by their populations g_J, as shown in Eq. (5),

$$\sigma_T(E) = \frac{g_{3/2}\sigma_0(E-E_T)^n + g_{1/2}\sigma_0(E+E_{1/2}-E_T)^n}{E^m}. \tag{5}$$

Here, $E_{1/2}$ is the energy of the $J=1/2$ excited state. A 2:1 statistical population is assumed, so that $g_{3/2}=2/3$ and $g_{1/2}=1/3$. Equal reactivity is assumed for each spin–orbit state since the same σ_0 is used.

The reaction cross section for an endothermic process may decline at higher energies due to dissociation of the product ion. For such systems, cross sections are analyzed using a model previously outlined, which makes a simple statistical assumption within the constraints of angular momentum conservation.[37] This model yields Eq. (6), a modified form of Eqs. (4) or (5), where P_D is the probability for dissociation of the product ion

$$\sigma(E) = \sigma_T[1-P_D]. \tag{6}$$

P_D is a function of both E_D, the energy at which dissociation begins, and p, a quantity related to the number of internal modes in the transition state. Thus for $E < E_D$, P_D is zero,

and for $E > E_D$, P_D asymptotically approaches one. For exothermic reactions, cross sections generally have a power law functional form, $\sigma_0 E^{-x}$, as in the LGS model [Eq. (2)]. Hence, dissociation channels for such processes can be modeled through Eq. (7),

$$\sigma(E) = \sigma_0 E^{-x}[1 - P_D]. \quad (7)$$

For endothermic reactions, optimized values of E_T, σ_0, and n are obtained by using nonlinear least-squares regression analysis to give the best fit to the data, after convoluting over the known ion beam and neutral energy distributions. In most cases, the data is fit with Eqs. (4) or (5) from below threshold up to energies where dissociation can begin E_D. Equation (6) is used for endothermic processes where E_T is close to E_D, since product dissociation can have a significant effect on the shape of the threshold region of the cross section and the optimum E_T. In the application of Eqs. (6) or (7) for exothermic reactions, E_D is either specified as the derived threshold energy for the dissociative channel or is iteratively optimized. The parameter p is treated as a variable but is limited to integer values. In each threshold determination, several data sets taken at different times and under different experimental conditions are analyzed. The uncertainties in E_T reported here include one standard deviation of the averge value and the absolute uncertainty in our energy scale, 0.05 eV (lab).

Another complication in threshold determination arises in highly endothermic product channels that rise slowly from threshold. Under such conditions, the threshold analysis above does not provide an unambiguous threshold energy. Therefore, we take the apparent threshold to be representative of the true threshold energy for such processes. This is reasonable since the broadening due to experimental energy distributions has little effect on the appearance of slowly rising cross sections.

RESULTS

$Ar^+ + SiF_4$

In the reaction of Ar^+ with SiF_4, processes (1a) through (1d) are observed. The resulting cross sections, shown in Fig. 1, reveal that SiF_3^+ formation is significantly favored at nearly all energies studied here. Although process (1e) is energetically accessible (Table II) no Si^+ product is observed, nor is ArF^+. Thus the cross section for these processes must be less than 0.01 Å^2. At low energies, the 60% uncertainty in the total cross section magnitude encompasses σ_{LGS} calculated with both $\alpha(SiF_4) = 3.32$ and 4.3 Å^3. At 2 eV, the cross section is approximately equal to $\sigma_{HS} \simeq 38$ Å^2; but by 50 eV, Ar^+ reacts in only one of about every four hard-sphere collisions. Thus, reaction occurs on nearly every collision until ~2 eV, and then the reaction efficiency declines monotonically with increasing energy.

The $SiF_4^+ + Ar$ cross section increases monotonically as the energy decreases, which indicates an exothermic process. Yet as shown in Fig. 2, the cross section behavior is more complicated than that usually observed for such processes.[27,38] Specifically, the cross section initially declines as $E^{-1.3 \pm 0.2}$, levels off between ~0.05 and ~0.2 eV, and then virtually resumes the original fall off function, $E^{-1.0 \pm 0.2}$.

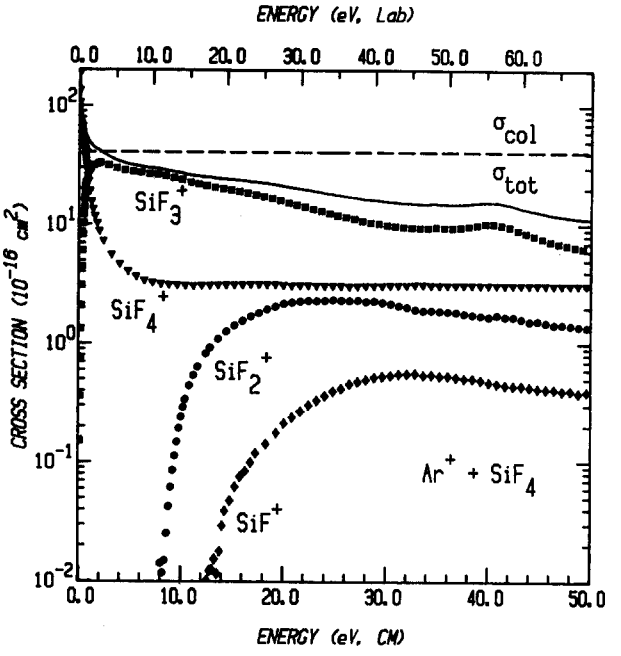

FIG. 1. Variation of product cross sections with translational energy in the laboratory frame of reference (upper scale) and the center-of-mass frame (lower scale) for reaction of Ar^+ with SiF_4, processes (1a) through (1d). The solid line shows the total reaction cross section. The dased line shows the collision cross section, given by the maximum of either the hard-sphere or LGS [$\alpha(SiF_4) = 3.32$ Å^3] cross sections, Eqs. (2) and (3).

This behavior, which is reproducible under all experimental conditions studied, is consistent with multiple spin–orbit states in the Ar^+ ion beam. SiF_4^+ production from $Ar^+(^2P_{3/2})$ is endothermic by 0.05 ± 0.02 eV (Table II), while production from $Ar^+(^2P_{1/2})$ is exothermic by

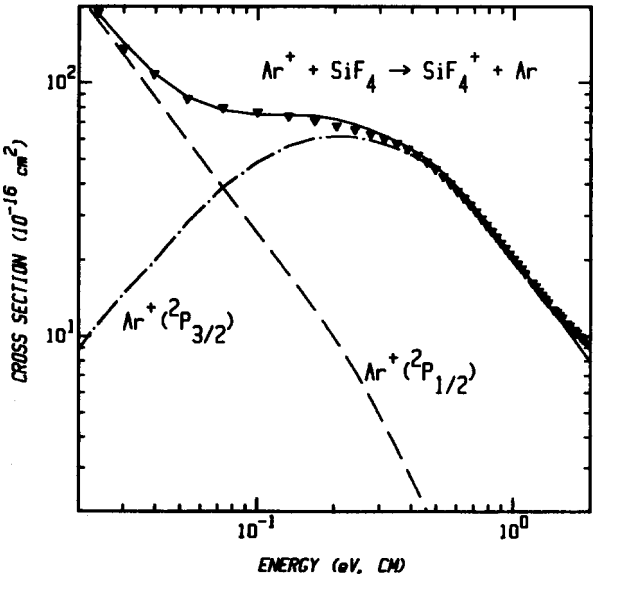

FIG. 2. Low energy region of the SiF_4^+ cross section from reaction of Ar^+ with SiF_4, process (1a). The dash–dot line shows the threshold fit of the $Ar^+(^2P_{3/2})$ feature using Eq. (6) with $E_T = 0.06$, $E_D = 0.43$, $p = 0$, $n = 0.57$, and $\sigma_0 = 39.2$. The exothermic feature due to reaction of $Ar^+(^2P_{1/2})$ is represented by the dashed line, $\sigma = 1.25 E^{-1.3}$ with dissociation at $E_D = 0.2$ eV included as in Eq. (7). The solid line shows the sum of these two fits.

0.13 ± 0.02 eV. Reliable analysis of the endothermic feature requires the use of Eq. (6), since dissociation of SiF_4^+ to $SiF_3^+ + F$ can begin less than 1 eV above the threshold (Table II). Here, we take E_D to be the threshold energy determined for the SiF_3^+ cross section as discussed below, $E_T(SiF_3^+) = 0.43 \pm 0.04$ eV. Optimization of parameters n, σ_0, and p result in excellent fits in the energy range 0.4 to 1.5 eV when $p = 0$, $n = 0.4$ to 0.7, $\sigma_0 = 38$ to 40, and $E_T = 0.03$ to 0.09 eV. These upper and lower limits on E_T are in good agreement with the expected value. From 0.02 to 1.5 eV, the SiF_4^+ cross section is modeled by the sum of the endothermic model and the exothermic model of Eq. (7), $1.25\,E^{-1.3\pm0.2}$ with $p = 0$ and $E_D = 0.2$. This value for E_D is in reasonable agreement with the expected threshold for dissociation of SiF_4^+, $0.43 - 0.178 = 0.25$ eV. Beyond ~ 8 eV, the SiF_4^+ cross section becomes constant with a magnitude of 3 Å^2, as shown in Fig. 1. This implies that in this energy range the SiF_4^+ is most likely produced through long-range electron transfer from Ar^+ that leaves very little internal energy in the SiF_4^+.

The SiF_3^+ cross section, process (1b), is slightly endothermic and reaches a maximum value of 3 Å^2 at ~ 2 eV. A threshold analysis of three data sets from 0.1 to 2 eV using Eq. (5) results in an excellent fit to the data, shown in Fig. 3, where $E_T = 0.43 \pm 0.04$ eV, $n = 0.85 \pm 0.02$, and $\sigma_0 = 43.2$. Although this value of E_T is lower than the value in Table II by 0.17 eV, the discrepancy lies within the 0.2 eV uncertainty. At higher energies, the SiF_3^+ cross section is nearly constant. The changes in shape (Fig. 1) are believed to be experimental artifacts, since these features are not reproducible and are dependent upon experimental conditions

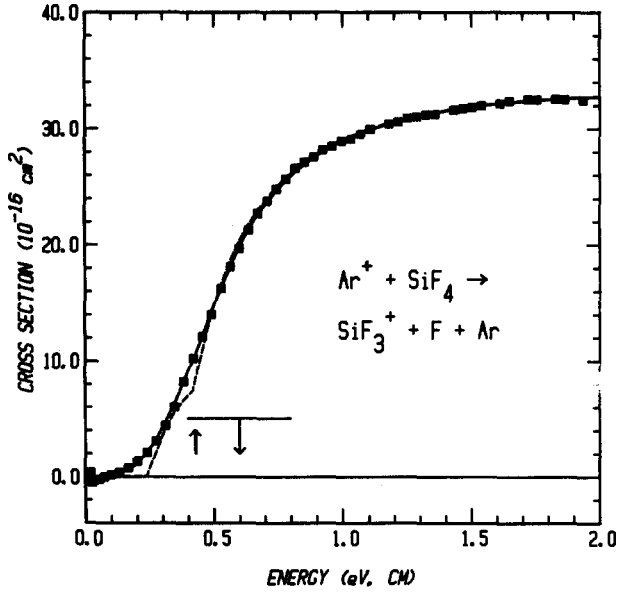

FIG. 3. Threshold region of SiF_3^+ production from Ar^+, process (1b). The dashed line shows the threshold fit calculated by using Eq. (5) with $E_T = 0.43$ eV, $n = 0.86$, and $\sigma_0 = 43.2$. This derived threshold energy for the $Ar^+(^2P_{3/2})$ state is shown by the upward arrow, and the literature value with error bar is shown by the downward arrow. The discontinuity in the dashed line is due to inclusion of both the $^2P_{3/2}$ and $^2P_{1/2}$ states of reactant Ar^+. The solid line shows the threshold model convoluted over the ion beam and neutral energy distributions.

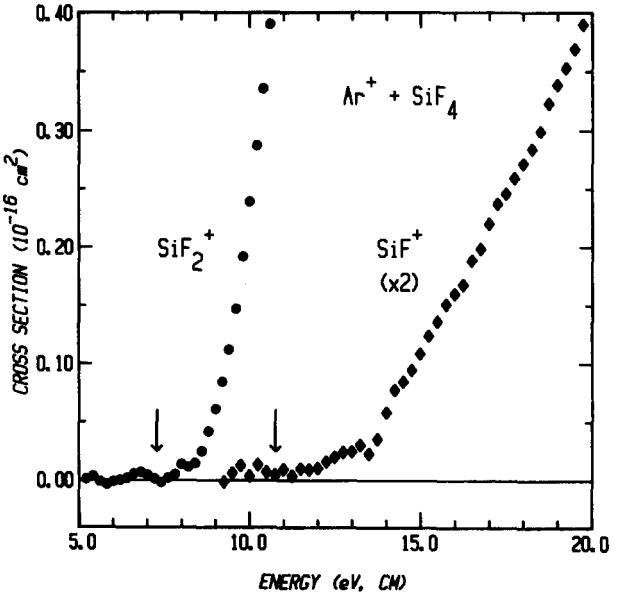

FIG. 4. Threshold regions of the SiF_2^+ (circles) and SiF^+ (diamonds) cross sections from reaction of $Ar^+ + SiF_4$, processes (1c) and (1d). The arrows indicate the literature thresholds for loss of F atoms: 7.3 and 10.8 eV, respectively.

as discussed above in the experimental section.

Reaction channels (1c) and (1d) are both highly endothermic processes. For SiF_2^+ production, process (1c), Fig. 4 indicates an apparent threshold at ~ 8 eV. This is roughly consistent with the expected threshold for formation of $SiF_2^+ + 2F$, 7.29 ± 0.09 eV (Table II). As can be seen from Fig. 1, the SiF_2^+ cross section reaches a maximum value of 2.3 Å^2 at ~ 25 eV, and then falls off with energy as $E^{-0.9}$. The threshold region for the final product ion observed, SiF^+ from process (1d), is also shown in Fig. 4 and has an apparent threshold at ~ 11 eV. This is near the expected threshold of 10.77 ± 0.10 eV for production of $SiF^+ + 3F$ (Table II).

$Ne^+ + SiF_4$

In the reaction of Ne^+ with SiF_4, processes (1b) through (1e) are observed, and the resulting cross sections are shown in Fig. 5. As in the Ar system, the rare gas fluoride ion, NeF^+, is not observed. At 0.05 eV, the LGS cross section calculated with $\alpha(SiF_4) = 3.3$ Å^3 is toward the upper edge of the error limits in the observed total cross section. Beyond 5 eV, the reactivity is approximately constant, and reaction occurs in about one of every three to four hard-sphere collisions. Comparison of the relative cross section magnitudes shows that the exothermic process, SiF_3^+ formation, dominates until 8 eV. At higher energies, the SiF_3^+, SiF_2^+, and SiF^+ cross sections are aproximately equal in magnitude, although SiF^+ predominates slightly. The rising Si^+ cross section becomes comparable to these other channels at the highest energies.

Formation of SiF_4^+, process (1a), was observed with a cross section function virtually identical in shape to that from the Ar^+ reaction (1a) above. However, the absolute magnitude was much smaller and varied widely from data

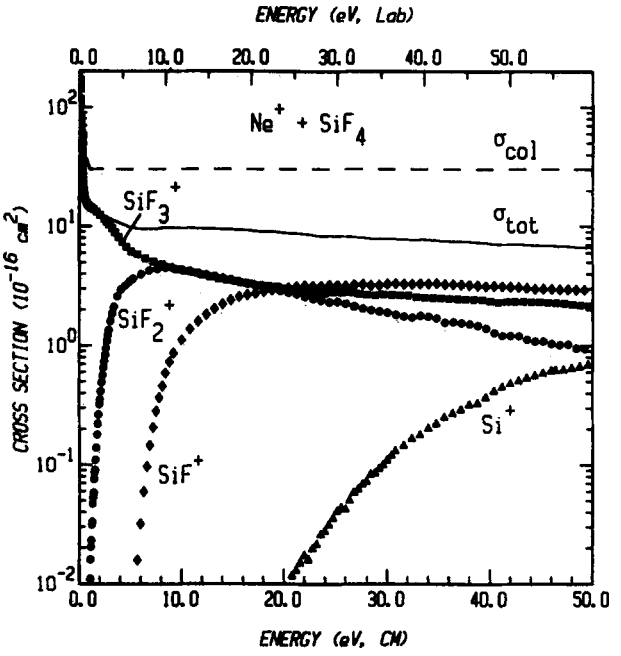

FIG. 5. Variation of product cross sections with translational energy in the laboratory frame of reference (upper scale) and the center-of-mass frame (lower scale) for reaction of Ne^+ with SiF_4, processes (1b) through (1e). The solid line shows the total reaction cross section. The dashed line shows the collision cross section, given by the maximum of either the hard-sphere or LGS [$\alpha(SiF_4) = 3.32$ Å^3] cross sections, Eqs. (2) and (3).

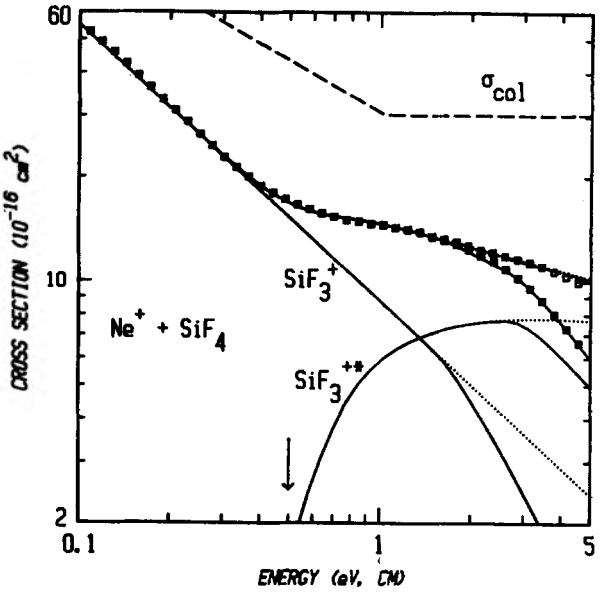

FIG. 6. The low energy region for the reaction of Ne^+ with SiF_4. The open squares show σ_{tot}, equivalent to the sum of $\sigma(SiF_3^+)$ and $\sigma(SiF_2^+)$, while solid squares show $\sigma(SiF_3^+)$ alone. The dashed line shows the collision cross section, given by the maximum of either the hard-sphere or LGS [$\alpha(SiF_4) = 3.32$ Å^3] cross sections, Eqs. (2) and (3). Other lines show the calculated cross sections for the postulated deconvolution of the cross section into ground and excited state processes. The line labeled SiF_3^+ shows the model for production of ground state SiF_3^+, $\sigma = 8.74\,E^{-0.8}$. The effect of dissociation into $SiF_2^+ + F$ is accounted for by Eq. (7), with $p = 0$ and $E_D = 1.57$ eV. The cross section attributed to excited state SiF_3^+* production is shown by the appropriately labeled line, and is modeled using Eqs. (5) and (6) with $E_T = 0.5$ eV, $n = 0.86$, $\sigma_0 = 10.6$, $E_D = 2.75$ eV, and $p = 0$. The arrow denotes the derived threshold energy. Both calculations are convoluted over the experimental energy distributions, and are summed to give the line running through the data points for $\sigma(SiF_3^+)$. The calculation of each model without inclusion of the dissociation process is shown by the dotted lines, and the dotted line running through the open squares depicts their sum.

set to data set. No correlation was found between the magnitude of this product and any experimental parameters, including reactant pressure, octopole power, electron energy, quadrupole resolution, and detection and focusing conditions. We believe that the explanation for this behavior is contamination by an impurity ion of $m/e = 20$ in the $^{20}Ne^+$ beam. Such an impurity has been previously observed,[39] and although not positively identified it is believed to be $^{40}Ar^{++}$. Another possible explanation, however, is that the SiF_4^+ product channel is severely affected by the ion collection difficulties discussed in the experimental section above. In each data set, the observed $\sigma(SiF_4^+)$ magnitude above 3 eV is virtually constant with energy and does not exceed 0.2 Å^2. Under the most controlled and reliable conditions, the magnitude above 3 eV was lower than the detection limit in this study, 0.01 Å^2, and at 0.1 eV the magnitude was less than 0.1 Å^2. In either case, the observed SiF_4^+ cross section is much smaller than those of processes (1b) through (1e). We believe the observation of this product is an experimental artifact, and thus it is not included in Fig. 5 nor considered further here.

The cross section for the SiF_3^+ product shows exothermic behavior as expected from the thermochemistry in Table II. Closer examination of the cross section at low energies in Fig. 6 shows rather atypical behavior for exothermic ion–molecule reactions.[27,38] Initially, $\sigma(SiF_3^+)$ declines with increasing energy as $E^{-0.80 \pm 0.07}$ from 0.02 to 0.4 eV, and then the cross section decreases much more slowly at higher energies. The low energy behavior, which decreases slightly faster than predicted by LGS in Eq. (2), $E^{-0.5}$, is clearly due to exothermic production of ground state SiF_3^+ (Table II). One explanation for the change in behavior at ~0.4 eV is that $\sigma(SiF_3^+)$ is mimicking the behavior of the collision cross section for charge transfer reactions. As discussed above, σ_{col} is initially represented by the LGS model, but then most likely levels off to the hard-sphere limit. This change occurs near the energy at which $\sigma(SiF_3^+)$ also levels off, which implies an approximately constant reaction efficiency. An alternative explanation for this behavior is that the cross section is really the sum of two independent processes: an exothermic one (which continues to decline as $E^{-0.8}$ until dissociation becomes important) and an endothermic process (which has an apparent threshold of ~0.4 eV). This latter feature could be due to production of an excited state of SiF_3^+.

SiF_2^+ production, process (1c), is clearly endothermic with an apparent threshold of ~1 eV. This is strong evidence that formation of molecular fluorine is not a significant process, since $SiF_2^+ + F_2$ is an exothermic channel (Table II). Analysis of the threshold region of the cross section, from 0.2 to 3.3 eV, with Eq. (5) results in $E_T = 0.8 \pm 0.1$ eV and $n = 3.2 \pm 0.1$. This is an exceedingly large value of n compared to others obtained in this study, 0.4 to 1.3, and in previous studies.[10,27,33,39] This value of E_T is 0.7 eV lower

than the expected threshold for $SiF_2^+ + 2F$ production, 1.48 ± 0.09 eV. This discrepancy could be due to reaction of the impurity in the Ne^+ beam discussed above; however, the probable cause of this anomalously low threshold is due to the inadequacies of Eq. (5) in dealing with two overlapping channels for SiF_2^+ production. As detailed below for the two features observed in the SiF_3^+ cross section, SiF_3^+ and SiF_3^+* dissociate to SiF_2^+ at different energies. Thus, the SiF_2^+ cross section produced from both SiF_3^+ and SiF_3^+* can be modeled by subtracting the endothermic and exothermic models calculated with dissociation included from those calculated without dissociation included. This procedure yields a cross section for SiF_2^+ formed from SiF_3^+* that has a threshold at ~2.5 eV and mimics the overall SiF_2^+ cross section behavior and magnitude from 2.5 to 3.5 eV. On the other hand, the resultant cross section for SiF_2^+ formed from ground state SiF_3^+ has a threshold near the thermodynamic limit and a much smaller magnitude. These two cross sections each rise rapidly from threshold (consistent with lower values of n), yet the sum rises slowly and with much curvature, which is consistent with the overall SiF_2^+ cross section observed.

Processes (1d) and (1e) are highly endothermic. The reaction cross section for the SiF^+ product, shown in Fig. 7, has an apparent threshold of ~5 eV. This is consistent with the expected threshold of 4.97 ± 0.10 eV (Table II) for $SiF^+ + 3F$ formation. The Si^+ product channel (1e) shows an apparent threshold at ~16 eV in Fig. 7, which exceeds the expected threshold for $Si^+ + 4F$ of 11.28 ± 0.04 eV by nearly 5 eV. This is not surprising, since this process involves successive loss of F atoms. In such processes, the probability is low that each F atom will depart with no momentum and leave all the interaction energy available for further dissociation. Thus, a kinetic shift is observed.

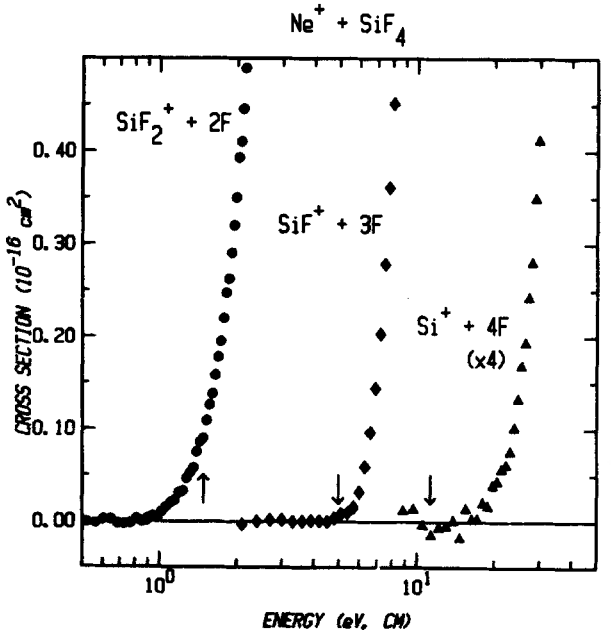

FIG. 7. Threshold regions of the SiF_2^+ (circles), SiF^+ (diamonds), and Si^+ (triangles) cross sections from reaction of $Ne^+ + Si_4$, processes (1c), (1d), and (1e). The arrows indicate the literature thresholds for loss of F atoms: 1.5, 5.0, and 11.3 eV, respectively.

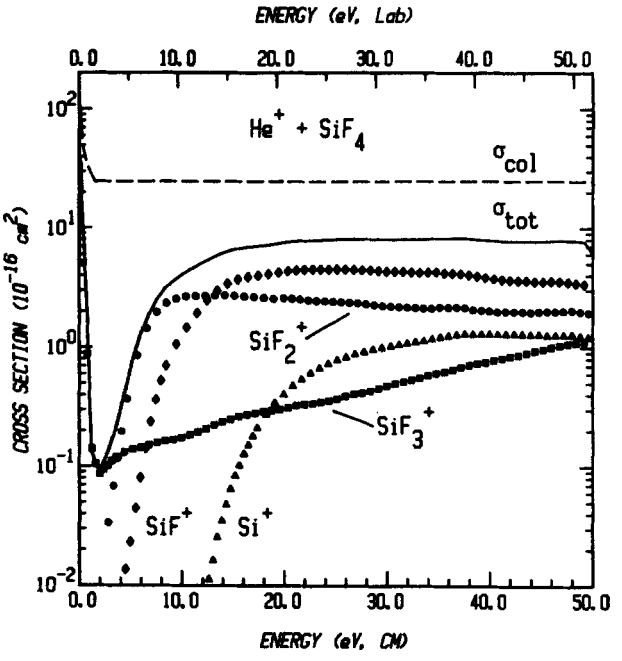

FIG. 8. Variation of product cross sections with translational energy in the laboratory frame of reference (upper scale) and the center-of-mass frame (lower scale) for reaction of He^+ with SiF_4, processes (1b) through (1e). The solid line shows the total reaction cross section. The dashed line shows the collision cross section, given by the maximum of either the hard-sphere or LGS [$\alpha(SiF_4) = 3.32$ Å^3] cross sections, Eqs. (2) and (3).

$He^+ + SiF_4$

Shown in Fig. 8 are the observed cross sections for the reaction of He^+ and SiF_4, processes (1b) through (1e). HeF^+ is not observed in the energy range studied here. The overall reaction is extremely inefficient at low energies, but from 15 to 50 eV, He^+ reacts about one of every three hard-sphere collisions. At most energies, SiF^+ formation dominates, and SiF_3^+ formation is the least efficient of these processes. However, the cross section magnitudes of channels (1c) through (1e) are within 60% of the SiF^+ magnitude at the highest energies.

As in the Ne^+ system, the cross section magnitude for SiF_4^+, process (1a), varied widely between data files from $< 10^{-2}$ to 10^{-1}, but here the shape of the cross section function also differed. Again, no correlation was found between the observed cross section and any specific parameters. Contamination in the ion beam may be responsible for this behavior, as believed for the Ne^+ reaction, but the identity of such an impurity is not apparent. Thus, the more likely explanation is that the SiF_4^+ product channel is subject to the difficulties associated with charge transfer processes discussed above. As is the case of the Ne^+ results, under the most controlled and reliable conditions, the magnitude of the SiF_4^+ cross section is lower than the detection limit in this study, 0.01 Å^2. Thus it is not included in Fig. 8 nor considered further here.

Process (1b), SiF_3^+ production, is exothermic by over 8 eV (Table II). One feature in the SiF_3^+ cross section shows endothermic behavior with a threshold at ~1 eV and is quite reproducible. Another feature is an exothermic channel that

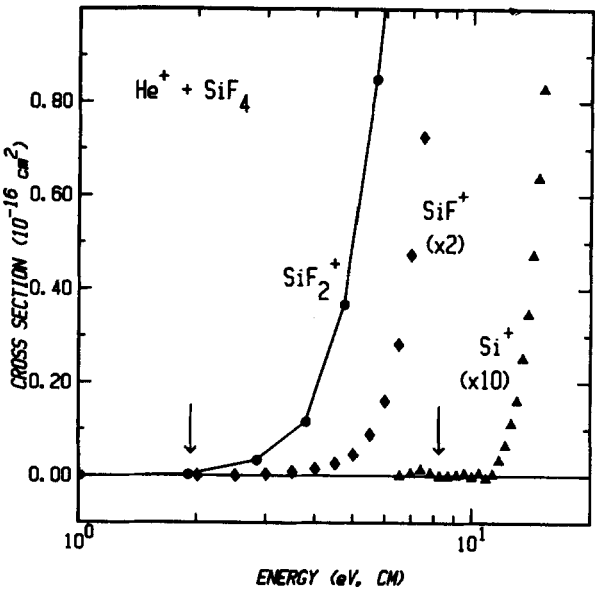

FIG. 9. Threshold regions of the SiF_2^+ (circles), SiF^+ (diamonds), and Si^+ (triangles) cross sections from reaction of He^+, processes (1c), (1d), and (1e). The arrows indicate the literature thresholds for $SiF^+ + 3F$ and $Si^+ + 4F$: 1.9 and 8.3 eV, respectively. Literature thermochemistry indicates that SiF_2^+ production is exothermic.

falls off very steeply as $E^{-3.2\pm0.6}$. This type of energy dependence is unusual, and the magnitude of this feature varied from <0.01 to 2 Å^2 at 0.5 eV with no correlation to specific experimental parameters. Thus it is likely to be an experimental artifact, which we believe is due to nonreactive radial scattering of the reactant ions. These scattered He^+ ions can be accelerated by the potential on the octopole rods, and react upon further collision at anomalously high energies. Thus reaction can be erroneously observed at low interaction energies, which is consistent with the behavior observed here. Only light reactant ions such as He^+, at low energies are subject to strong radial scattering and this effect. At energies higher than ~ 1 eV and for heavier reactant ions, this effect is not in evidence.

Although the SiF_2^+ channel, reaction (1c), is expected to be exothermic by 1.54 ± 0.09 eV (Table II), the SiF_2^+ cross section shows an apparent threshold of ~ 2 eV. The final two reaction channels observed in the reaction of $He^+ + SiF_4$ are formation of SiF^+ and Si^+, processes (1d) and (1e). The threshold regions of these reaction cross sections are shown in Fig. 9. Both are expected to be endothermic, but the apparent thresholds of 3 eV for SiF^+ and 11 eV for Si^+ are 1 and 3 eV higher, respectively, than expected for F atom formation (see Table II).

DISCUSSION

F_2 versus 2 F loss

Although loss of F_2 is energetically favored over loss of two F atoms, the latter is most likely the dominant, and possibly the exclusive, process occurring. Strong evidence for this is provided by the observed endothermic behavior for SiF_2^+ production from Ne^+, since the $SiF_2^+ + F_2$ channel is expected to be exothermic. Further experimental evidence for preferred loss of 2 F lies in the fact that the SiF^+ cross section from Ne^+ and the Si^+ and SiF^+ cross sections from Ar^+ have apparent thresholds that coincide with F atom production. Loss of F atoms is expected to be kinetically favored, since it proceeds through a loose transition state and can more readily conserve angular momentum than formation of F_2, which requires a tight transition state.

General behavior and relative reactivity

Similarities are found in the general behavior of the Ar, Ne, and He systems. First production of the rare gas fluoride ion is not observed in any of the three systems. Second, the reaction cross sections do not decline rapidly at high energies, which implies that the SiF_x^+ products contain little internal energy that would otherwise cause dissociation into the SiF_{x-1}^+ species. The excess energy must instead be placed in translational modes of the Rg, F, or SiF_x^+ products. This is consistent with charge transfer processes which occur with large impact parameters.

The Ne and He results show additional similarities. At energies above 20 eV, the SiF^+ product is dominant, and SiF_4^+ is not observed. In the Ar system, on the other hand, SiF_4^+ is a significant product, the SiF^+ channel has the smallest cross section observed, and the Si^+ product is not seen at all. At high energies, the He and Ne results show the SiF_3^+, SiF_2^+, SiF^+, and Si^+ cross sections have approximately the same magnitude, all within a factor of ~ 4. Yet in the Ar system, SiF_3^+ production is favored over any other process by factors ranging from 5 to 16. The explanation for this behavior is based on thermodynamic grounds. With Ar, charge transfer is a slightly endothermic process, so that very little excess energy is available for dissociation. Furthermore, after successive loss of F atoms, the probability is very low that enough excess energy will be present in SiF^+ to produce Si^+. With He and Ne, on the other hand, the excess energy is such that virtually all the SiF_4^+ formed dissociates. Even after the loss of three F atoms, enough internal energy remains in SiF^+ for dissociation into Si^+. In all three systems, the first process that is significantly endothermic dominates the reactivity above several volts of collision energy. This process is SiF^+ formation for He and Ne, and SiF_3^+ for Ar.

The cross sections at low energies in the $He^+ + SiF_4$ system do not behave consistently with either the Ne or Ar results. Specifically, all processes (1b) through (1e) fail to show significant cross sections until well above the thermodynamic limits, thus indicating reaction barriers. Such behavior has also been observed in simpler systems involving He^+ and Ne^+, such as reaction with molecular hydrogen.[39] The observed barriers in the $Rg^+ + H_2$ reaction channels are easily explained by examination of the potential energy surfaces, as originally introduced by Mahan.[40] Here, only the $[H_2^+ + Rg]$ surface correlates with the ground state product surface, $[RgH^+ + H]$, while the reactant $[Rg^+ + H_2]$ surface correlates with production of an excited hydrogen atom, $[RgH^+ + H^*]$. Thus additional energy is needed to produce the excited state.

Construction of potential energy surfaces

As in the He^+, $Ne^+ + H_2$ systems, insight into the dynamics and relative reactivities of the present systems can be obtained by constructing potential energy surfaces (PESs). The following treatment is far from quantitative, but is designed to elucidate the important qualitative features in these reactions. Formation of SiF_x^+ products begins with charge transfer from Rg^+ to form SiF_4^+. Thus the region of interest is the crossing from the $[Rg^+ + SiF_4]$ surface to a $[SiF_4^+ + Rg]$ surface. The $SiF_3 + F + Rg^+$ channel correlates with $SiF_4 + Rg^+$ along an attractive, bonding surface that corresponds to a spin-paired interaction between SiF_3 and F. Likewise, $SiF_3^+ + F + Rg$ correlates with $SiF_4^+ + Rg$ along such an attractive surface. Also of interest here is the repulsive, antibonding $[SiF_3^+\text{–}F + Rg]$ surface that arises from the spin-aligned interaction of SiF_3^+ and F.

Treatment of $SiF_3\text{–}F^{(+)}$ as a diatomic species simplifies the construction of these surfaces, and still illustrates the dominant behavior. The contour of each surface then is dependent upon the equilibrium internuclear distance r_e and the well depth D_e for the approximated diatomic species $SiF_3\text{–}F^{(+)}$. MNDO calculations indicate that $r_e(SiF_4^+)$ exceeds $r_e(SiF_4)$ by only 1.2%.[41] The value $r_e(SiF_4) = 1.552 \pm 0.002$ Å has been measured,[23] and increasing this value by 1.2% yields $r_e(SiF_4) = 1.57$ Å. The well depth D_e is the sum of the dissociation energy, determined from the thermochemistry in Table I, and the zero-point energy. Value used for D_e are 6.46 eV for SiF_4 and 0.55 eV for SiF_4^+. For each Rg system, the minimum of the $[Rg^+ + SiF_4]$ surface is offset from that of the $[SiF_4^+ + Rg]$ surface by the difference between IP(Rg) and IP(SiF_4), which is given in Table II as the threshold for process (1a). The attractive, bonding $SiF_3\text{–}F^{(+)}$ surfaces are calculated using a Morse potential[42] with $\omega_e(SiF_3\text{–}F) = 1400$ cm^{-1},[43] and $\omega_e(SiF_3^+\text{–}F) = 900$ cm^{-1}.[44] For the $SiF_3^+\text{–}F + Rg$ channel, this Morse potential is nearly identical to a calculated bonding surface for H_2^+[45] when scaled to the proper r_e and D_e of $SiF_3^+\text{–}F$ (1.57 Å and 0.55 eV). This is not surprising since the $SiF_3^+\text{–}F$ bond involves only one electron, as in H_2^+. Thus, a reasonable approximation to the $[SiF_3^+\text{–}F + Rg]$ repulsive, antibonding surface is provided by an identical scaling of the H_2^+ antibonding surface.[45]

Analysis of potential energy surfaces

An explanation for the observed reactivity is provided by the resulting potential surfaces. These are shown in Figs. 10, 11, and 12 for infinitely separated reactants in the Ar, Ne, and He systems, respectively. Notice that the vertical scales of these diagrams differ appreciably, a result of the very different rare gas ionization potentials. In each case, the reaction coordinate lies in the bottom of the $Rg^+ + SiF_4$ well and is orthogonal to the plane of the diagram. Reaction requires that the reactants move from this SiF_4 well to the seam connecting the $[Rg^+ + SiF_4]$ and $[SiF_4^+ + Rg]$ surfaces. For the Ar system in Fig. 10, the PESs shows extensive overlap between the these surfaces, such that the surface crossing seam is near the equilibrium geometry of the SiF_4

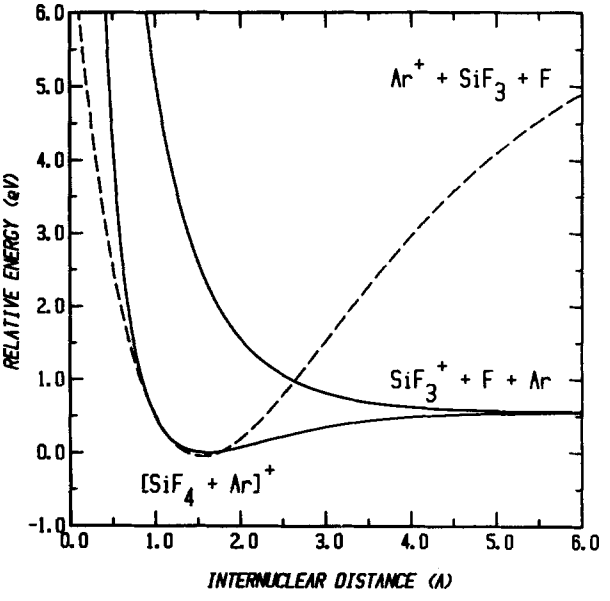

FIG. 10. Qualitative potential energy surfaces for the $[Ar + SiF_4]^+$ system. The dashed line represents the interaction of $F_3Si\text{–}F$, while the solid lines represent the interactions of $F_3Si^+\text{–}F$. The energy zero is shown as the zero point energy of bound SiF_4 and corresponds to the energy of the $Ar^+ + SiF_4$ reactants. The energy separation between the zero point energies of SiF_4 and SiF_4^+ is the reaction endothermicity for process (1a) from Table II, 0.05 eV.

reactant well. Electron transfer to form SiF_4^+ is therefore a near-resonant process, so that the reaction is highly efficient and proceeds without barrier. For the Ne system, Fig. 11, the $[Ne^+ + SiF_4]$ surface crosses the higly repulsive regions of the bound and unbound $[SiF_3^+\text{–}F + Ne]$ surfaces. This ex-

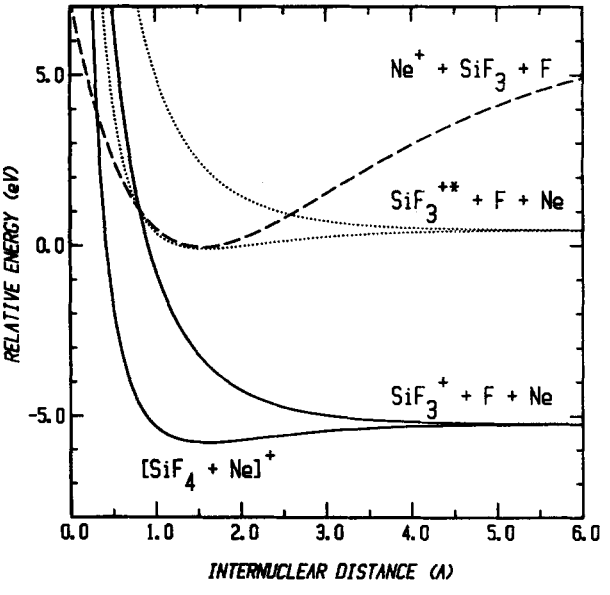

FIG. 11. Qualitative potential energy surfaces for the $[Ne + SiF_4]^+$ system. The dashed line represents the interaction of $F_3Si\text{–}F$, and the solid lines represent the interactions of $F_3Si^+\text{–}F$. The energy zero is shown as the zero point energy of bound SiF_4 and corrresponds to the energy of the $Ne^+ + SiF_4$ reactants. The energy separation between the zero point energies of SiF_4 and ground state SiF_4^+ is the reaction exothermicity for process (1a) from Table II, 5.8 eV. The dotted lines represent the interactions of excited state $F_3Si^{+*}\text{–}F$. The energy separation between the solid and dotted lines is the excited state energy of 5.7 eV.

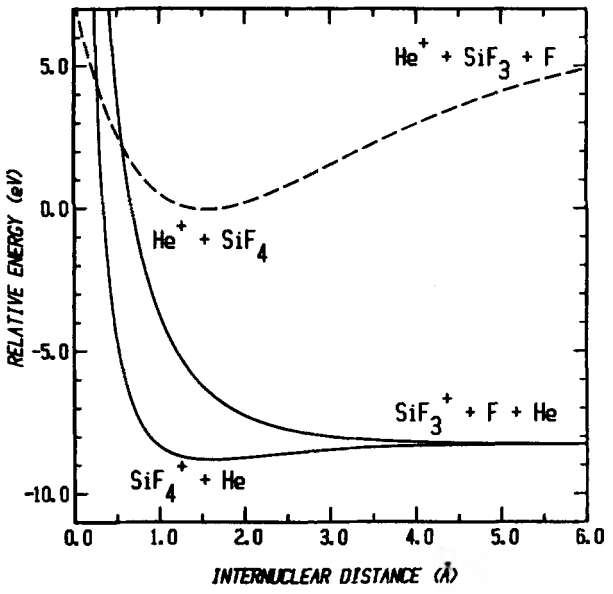

FIG. 12. Qualitative potential energy surfaces for the $[He + SiF_4]^+$ system. The dashed line represents the interaction of F_3Si–F, while the solid lines represent the interactions of F_3Si^+–F. The energy zero is shown as the zero point energy of bound SiF_4 and corresponds to the energy of the $He^+ + SiF_4$ reactants. The energy separation between the zero point energies of SiF_4 and SiF_4^+ is the reaction exothermicity for process (1a) from Table II, 8.8 eV.

plains why no SiF_4^+ is observed. Furthermore, since no barrier is observed in the SiF_3^+ product channel, the point at which the system crosses from the $[Rg^+ + SiF_4]$ surface to the $[SiF_4^+ + Rg]$ surface must lie below the energy of the reactants. Either the crossing actually occurs closer to the SiF_4 equilibrium bond distance than is shown in Fig. 11 or the ion-induced dipole attraction overcomes the small barrier (~ 1 eV) in this figure. More quantitative calculations could answer this more definitively. Finally, for the helium system, Fig. 12 shows that the reactant surface again crosses the highly repulsive parts of the $[SiF_3^+ + F + He]$ and $[SiF_4^+ + He]$ surfaces. This is again consistent with no SiF_4^+ being formed. Unlike the Ne system, however, the asymptotic energy of this surface crossing is ~ 2 eV. This is consistent with the observation that little if any reaction is observed until greater than about 1 eV of kinetic energy. Now the ion-induced dipole attraction is insufficient to overcome this barrier.

SiF_3^+ excited state

As discussed above, the SiF_3^+ cross section produced from Ne^+ undergoes a change in behavior near 0.4 eV. One explanation for this is production of an SiF_3^+* excited state that becomes energetically accessible at the translational threshold energy. Combining the exothermicity of process (1b) from Table II, 5.21 eV, with the approximate threshold for this process, $E_T = 0.4$ eV, implies that this excited state lies at ~ 5.6 eV. Support for this interpretation of the SiF_3^+ data is given by an earlier prediction of an SiF_3^+ excited state that, in analogy with BF_3, lies between 5 and 6 eV above the $^1A_1$ ground state.[46] Also the Ar^+ results do not show this type of cross section behavior, as might be expected if it were due solely to the behavior of σ_{col}. Further support is given by the PESs, since the excited state $[SiF_3^+$*$-F + Rg]$ surfaces would lie in a near resonance with the reactant $[He^+ + SiF_4]$ surface, as in the Ar system. Thus, the crossings between such surfaces would be efficient, consistent with the observance of a signifcant excited state feature in $\sigma(SiF_3^+)$.

To model the energy dependence of the endothermic excited state feature in $\sigma(SiF_3^+)$, the exothermic feature, $8.74E^{-0.8}$, is subtracted from the sum of $\sigma(SiF_3^+)$ and its dissociation product, $\sigma(SiF_2^+)$. Analysis of the remaining cross section yields the optimized parameters in Eq. (5) of $n = 0.86 \pm 0.05$, $E_T = 0.5 \pm 0.1$ eV, and $\sigma_0 = 10.6$. This value for E_T yields an excited state energy of 5.7 ± 0.1 eV. These optimized parameters are then used to model $\sigma(SiF_3^+)$ alone by incorporating dissociation in both the endothermic and exothermic features, Eqs. (6) and (7). Excellent fits to $\sigma(SiF_3^+)$ are obtained when E_D is 1.5 to 1.7 eV for the exothermic feature and 2.6 to 2.8 eV for the endothermic SiF_3^+* feature. The dissociative onset for SiF_3^+ coincides with the expected value of 1.48 ± 0.09 eV (Table II) for dissociation into SiF_2^+, but E_D for SiF_3^+* is ~ 1.2 eV higher than this thermodynamic limit. This would imply that dissociation of SiF_3^+* produces an excited state of SiF_2^+, or that the additional energy goes into translational modes of either ground state SiF_2^+ or the dissociated F atom. Figure 6 compares the data to the final models for production of both ground state and excited state SiF_3^+, with and without dissociative fall off.

Assuming that the proposed SiF_3^+* excited state is actually formed in the Ne^+ reaction, the implications of its presence on the observed reactivity can be discussed in terms of the PESs. Qualitative SiF_3^+*–F surfaces are estimated as the ground state surfaces shifted by 5.7 eV, shown in Fig. 11. This clearly exhibits the near-resonant nature of the $[Ne^+ + SiF_4]$ and $[SiF_3^+$*$-F + Ne]$ surfaces mentioned above. Since little if any SiF_4^+ is observed in the Ne system, any SiF_4^+* formed must have sufficient energy that it rapidly dissociates either to SiF_3^+* + F or to ground state SiF_3^+ + F via a crossing with the ground state $[SiF_3^+ + F + Ne]$ surface. In the Ar^+ results, no SiF_3^+* excited state features are observed. In this system, SiF_3^+* production would be highly unfavorable since a $\geqslant 5.7$ eV barrier would exist to crossing between the $[Ar^+ + SiF_4]$ and $[SiF_3^+$* $+ F + Ar]$ surfaces. For the He system, no definitive interpretation of the effect of the excited state surfaces on the observed reactivity is readily made due to the uncertainties involved. However, the observed exothermic feature in $\sigma(SiF_3^+)$ could be explained as production of SiF_3^+*, since our qualitative surfaces indicate that the unbound $[SiF_3^+$* $+ F + He]$ surface would cross near the $[He^+ + SiF_4]$ potential minimum.

Thermochemistry

The energy dependence in the reaction cross sections from the Ar and Ne systems is, in general, consistent with the literature thermochemistry and that derived in our previous work.[17] Production of SiF_4^+ from Ar^+ ($^2P_{3/2}$) shows a threshold between 0.03 and 0.09 eV, which is in good agree-

ment with the literature value of 0.05 ± 0.02 eV. Likewise the threshold for production of SiF_3^+ from $Ar^+(^2P_{3/2})$ is determined to be 0.43 ± 0.04 eV. This lies within the uncertainty of the literature value, 0.6 ± 0.2 eV, but is much more precise. This threshold yields $\Delta H^0_{f298}(SiF_3^+) = -30.1 \pm 0.9$ kcal/mol, as compared to the previously measured values of -30 ± 7,[47] -22 ± 5,[48] and -26.7 ± 4.5 kcal/mol.[17] Although production of SiF_2^+ and SiF^+ from Ar^+, and SiF^+ and Si^+ from Ne^+ are processes which might be subject to kinetic shifts, only the latter process has an apparent threshold significantly greater than the thermodynamic limit. The other processes show thresholds within 1 eV of the expected value. In the He^+ system, however, all thresholds are well in excess of their thermodynamic values, a result which is explained by the PES considerations.

Relation to plasma systems

To predict the optimum physical parameters of a plasma system, it is first necessary to understand the interactions at the substrate and ascertain the primary chemical species responsible for the desired deposition or etching process. Then the gas-phase chemistry can be tailored by modifying the starting materials and bias of the substrate to obtain the maximum concentration of reactive species. For instance, if SiF_3^+ (or products of SiF_3^+ reactions) were found to be particularly significant in the surface reactions which lead to etching of silicon layers, then the present results suggest that the use of Ar over Ne or He in the starting material would result in higher etch rates. Likewise, knowledge of the gas-phase reaction product distributions can rationalize experimental parameters which have been empirically determined. For instance, the use of Ar^+, along with XeF_2, results in a $\sim 25\%$ increase over Ne^+ and a fourfold increase over He^+ in the etch yields of Si layers.[8] SiF_4 is a primary etching product in these systems and will be present in significant amounts. Therefore, a hypothesis consistent with these results and the present work is that the larger SiF_x^+ species, or the neutral products of their reactions, can better assist the etching process than such species as Si^+ and SiF^+.

SUMMARY

Guided ion beam mass spectrometry has been used to study the reactions of Ar^+, Ne^+, and He^+ with SiF_4 from thermal energy to 50 eV c.m. Charge transfer followed by losses of atomic fluorine are the sole processes observed in each case. In the Ar system, processes (1a) through (1d) are observed, while in the He and Ne systems processes (1b) through (1e) are observed. The dominant process beyond several eV in each system is production of the first SiF_x^+ product which is significantly endothermic: SiF_3^+ for Ar^+, and SiF^+ for both Ne^+ and He^+. Therefore, product distributions of charge transfer processes involving the rare gas ions are significantly affected by the identity and ionization potential of the rare gas. At high energies, the cross sections decline slowly, which implies that only a small fraction of excess energy is left in internal modes.

In the Ar^+ and Ne^+ systems, the observed energetics are consistent with that expected from the literature. Both the exothermic reaction of $Ar^+(^2P_{1/2})$ and endothermic reaction of $Ar^+(^2P_{3/2})$ to produce SiF_4^+ are observed. From the SiF_3^+ cross section produced from Ar^+, the value $\Delta H^0_{f298} = -30.1 \pm 0.9$ kcal/mol is derived which agrees with the literature value, but has much lower uncertainty. In addition, there is some evidence that an excited state of SiF_3^+ is produced in the reaction with Ne^+. The data can be interpreted to indicate that such a state lies 5.7 eV above the ground state. For the He^+ reactions, all product channels observed show reaction barriers.

The reactivity and product distributions in the three systems can be explained using potential energy surfaces and reaction thermochemistry. Since formation of SiF_x^+ products begins with charge transfer from Rg^+ to form SiF_4^+, then the significant region on the potential surfaces is the crossing from the $[Rg^+ + SiF_4]$ surface to the $[SiF_3^+ - F + Rg]$ surfaces. The ionization potentials of Ar and SiF_4 are nearly equal, so that there is strong overlap between these surfaces. This explains why Ar^+ is highly reactive with SiF_4 and why no barrier is observed for reaction in this system. On the other hand, the ionization potential of He is nearly 9 eV greater than that of SiF_4. Thus, the crossing occurs at a small internuclear distance along the repulsive part of the $[He^+ + SiF_4]$ surface such that a barrier to reaction is observed. No SiF_4^+ formation is observed, which is consistent with the fact that the crossing occurs in the repulsive region of the $[SiF_3^+ - F + He]$ surfaces. The ionization potential of Ne lies intermediate between Ar and He and is 6 eV higher than that of SiF_4. Since no barrier to reaction is observed, the surface crossing of interest probably occurs near the minimum of the $[Ne^+ + SiF_4]$ bonding surface. However, the crossing occurs on the repulsive part of the $[SiF_3^+ - F + Ne]$ surface, as in the He system, so that no SiF_4^+ is produced from Ne^+ either. Finally, the plausibility that excited state SiF_3^{+*} is formed in the Ne system is reinforced by the PESs which show that the $[SiF_3^{+*} - F + Ne]$ surface would be nearly resonant with the $[Ne^+ + SiF_4]$ surface.

ACKNOWLEGEMENT

This work was funded by the Air Force Wright Aeronautical Laboratories.

[1] H. Chatham and A. Gallagher, J. Appl. Phys. **58**, 159 (1985).
[2] C. A. DeJoseph, Jr., P. D. Haaland, and A. Garscadden, IEEE Trans. Plasma Sci. **PS-14**, 165 (1986).
[3] G. Turban, Y. Catherine, and B. Grolleau, Plasma Chem. Plasma Process. **2**, 61 (1982); Thin Solid Films **67**, 309 (1980).
[4] J. C. Knights, R. A. Lujan, M. P. Rosenblum, R. A. Street, D. K. Bieglesen, and J. A. Reimer, Appl. Phys. Lett. **38**, 331 (1981).
[5] T. L. Chu, S. S. Chu, S. T. Ang, A. Duong, Y. X. Han, and Y. H. Liu, J. Appl. Phys. **60**, 4268 (1986).
[6] J. W. Coburn and H. F. Winters, J. Appl. Phys. **50**, 3189 (1979).
[7] Y. Tu, T. J. Chuang, and H. F. Winters, Phys. Rev. B **23**, 823 (1980).
[8] U. Gerlach-Meyer, J. W. Coburn, and E. Kay, Surf. Sci. **103**, 177 (1981).
[9] H. Chatham, D. Hils, R. Robertson, and A. C. Gallagher, J. Chem. Phys. **79**, 1301 (1983).

[10]B. H. Boo and P. B. Armentrout, J. Am. Chem. Soc. **109**, 3549 (1987).
[11]J. E. Parker and F. S. M. El-Ashhab, Int. J. Mass Spectrom. Ion Phys. **47**, 159 (1983).
[12]R. Richter and W. Lindinger, in Proceedings of the Fourth International Symposium of Atomic Surface Physics edited by F. Howorka, W. Lindinger, and T. D. Mark, Innsbruck, Austria, 1986, p. 202.
[13]J. Sasaki, I. Kuen, and F. Howorka, J. Chem. Phys. **86**, 1938 (1987).
[14]J. F. M. Aarts, Chem. Phys. Lett. **114**, 114 (1985).
[15]S. Fujita, T. Ohishi, H. Toyoshima, and A. Sasaki, J. Appl. Phys. **57**, 426 (1985).
[16]H. Boyd and M. S. Tang, Solid State Technol. **25**, 133 (1979).
[17]M. E. Weber and P. B. Armentrout, J. Chem. Phys. **88**, 6898 (1988).
[18]M. W. Chase, Jr., C. A. Davies, J. R. Downey, Jr., D. J. Frurip, R. A. McDonald, and A. N. Syverud, *JANAF Thermochemical Tables*, 3rd ed., J. Phys. Chem. Ref. Data **14**, Suppl. 1 (1985).
[19]G. Gioumousis and D. P. Stevenson, J. Chem. Phys. **29**, 294 (1958).
[20]E. W. Rothe and R. B. Bernstein, J. Chem. Phys. **31**, 1619 (1959).
[21]K. J. Miller and J. A. Savchik, J. Am. Chem. Soc. **101**, 7206 (1979).
[22]The calculation is based on the value $\alpha(SiH_4) = 4.339$ Å^3, taken from S. S. Batsonov, *Refractometry and Chemical Structure*, translated by P. P. Sutton (Consultants Bureau, New York, 1961).
[23]K. Hagen and K. Hedberg, J. Chem. Phys. **59**, 1549 (1973).
[24]M. Hottoka, B. Roos, J. B. Delos, R. Srivastava, R. B. Sharma, and W. S. Koski, Phys. Ref. A **35**, 4515 (1987).
[25]J. F. Liebman and L. C. Allen, J. Am. Chem. Soc. **92**, 3539 (1970).
[26]$r_e(ArH^+) = 1.28$ Å, $r_e(NeH^+) = 0.99$ Å, and $r_e(HeH^+) = 0.7743$ Å, taken from K. Huber and G. Herzberg, *Constants of Diatomic Molecules* (Van Nostrand Reinhold, New York, 1979).
[27]K. M. Ervin and P. B. Armentrout, J. Chem. Phys. **83**, 166 (1985).
[28]E. Teloy and D. Gerlich, Chem. Phys. **4**, 417 (1974).
[29]C. E. Moore, Natl. Stand. Ref. Data Ser., Natl. Bur. Stand. No. 34 (U.S. GPO, Washington, D. C., 1970).
[30]P. M. Hierl, V. Pacak, and Z. Herman, J. Chem. Phys. **67**, 2678 (1977).
[31]L. S. Sunderlin, K. M. Ervin, and P. B. Armentrout (unpublished work).
[32]K. M. Ervin and P. B. Armentrout, J. Chem. Phys. **84**, 6738 (1986).
[33]N. Aristov and P. B. Armentrout, J. Am. Chem. Soc. **108**, 1806 (1986); L. Sunderlin, N. Arisotov, and P. B. Armentrout, *ibid.* **109**, 78 (1987).
[34]W. J. Chesnavich and M. T. Bowers, J. Phys. Chem. **83**, 900 (1979).
[35]B. H. Boo and P. B. Armentrout, J. Phys. Chem. **91**, 5777 (1987).
[36]J. L. Elkind and P. B. Armentrout, J. Phys. Chem. **91**, 2037 (1987).
[37]M. E. Weber, J. L. Elkind, and P. B. Armentrout, J. Chem. Phys. **84**, 1521 (1986).
[38]J. D. Burley, K. M. Ervin, and P. B. Armentrout, Int. J. Mass Spectrom. Ion Process. **80**, 153 (1987).
[39]K. M. Ervin and P. B. Armentrout, J. Chem. Phys. **86**, 6240 (1987).
[40]B. H. Mahan, J. Chem. Phys. **55**, 1436 (1971); Acc. Chem. Res. **8**, 55 (1975).
[41]C. Glidewell, J. Mol. Struct. **85**, 87 (1981).
[42]G. Herzberg, *Molecular Spectra and Molecular Structure II. Spectra of Diatomic Molecules*, 2nd ed. (Van Nostrand Reinhold, New York, 1950), p. 101.
[43]If instead $\omega_e(SiF_3\text{–}F)$ is approximated as $\omega_e(SiF) = 857$ cm^{-1}, the resulting Morse potential is physically unrealistic.
[44]Here $\omega_e(SiF_3^+\text{–}F)$ is approximated as that of SiF^+. The value of 900 cm^{-1} has been previously estimated by analogy with CF/CF^+, $SiCl/SiCl^+$, and CCl/CCl^+ species (Ref. 17).
[45]D. A. McQuarrie, *Quantum Chemistry* (University Science Books, Mill Valley, California 1983), p. 358. For these solutions, the minimum in the H_2^+ potential surface yields $r_e(H_2^+) = 1.3$ Å, and the well depth yields $D_e(H_2^+) = 1.76$ eV.
[46]T. R. Hayes, R. J. Shul, F. A. Baiocchi, R. C. Wetzel, and R. S. Freund, J. Chem. Phys. **89**, 4035 (1988).
[47]J. D. McDonald, C. H. Williams, J. C. Thompson, and J. L. Margrave, Adv. Chem. Ser. **72**, 261 (1968).
[48]M. K. Murphy and J. L. Beauchamp, J. Am. Chem. Soc. **99**, 2085 (1977). This value differs from the originally reported value, since it is based on the revised $\Delta H^\circ_{f,298}(CH_3)$ of -34.82 ± 0.19 kcal/mol (Ref. 18) and is converted from the stationary electron convention.